Dynamical structure factor of a nonlinear Klein-Gordon lattice

Laurent Proville*

Service de Recherches de Métallurgie Physique, CEA-Saclay/DEN/DMN 91191-Gif-sur-Yvette Cedex, France
(Received 26 May 2005; revised manuscript received 8 September 2005; published 15 November 2005)

The quantum modes of a nonlinear Klein-Gordon lattice have been computed numerically [L. Proville, Phys. Rev. B **71**, 104306 (2005)]. The on-site nonlinearity has been found to lead to phonon bound states. In the present paper, we compute numerically the dynamical structure factor so as to simulate the coherent scattering cross section at low temperature. The inelastic contribution is studied as a function of the on-site anharmonicity. Interestingly, our numerical method is not limited to the weak anharmonicity and permits one to study thoroughly the spectra of nonlinear phonons.

I. INTRODUCTION

The scattering of neutrons,[1] x-rays,[2] and electrons[3] provides numerous insights into condensed matter and molecular physics. In particular, the inelastic scattering allows one to probe the dynamics of crystals and molecules. The dynamical structure factor, $S(q, \omega)$ which is proportional to the scattering cross section can be calculated by solving the Schrödinger equation for the lattice modes (within the Born approximation), so this quantity is essential for bridging theory to experiment. However the lattice eigenmodes may be figured out exactly only in the harmonic lattice model (see for instance Refs. 1 and 4) and thus the anharmonic contributions to the energy are neglected, although they stem from the atomic interaction potential. The standard harmonic treatment of lattice dynamics has well-known flaws in solids[5] and consequently, the discrete lattice anharmonicity has been a matter of intensive theoretical research in different contexts (for instance see Refs. 6–17). In order to examine the effect of anharmonicity on $S(q, \omega)$, some approaches have been attempted in different quantum lattice models, e.g., the Hubbard model for bosons[18,19] and the Klein-Gordon model with a weak on-site anharmonicity.[20] The latter is often quoted as nonlinear Klein-Gordon lattice (KG) and, noteworthy, it may account for the intrinsic anharmonicity of molecular crystals,[6,21–25] molecule bonds,[26,27] or metals where interstitial gaps are filled with light particles, as metal hydrides.[28–31] It is the reason why we proposed a numerical method[32] that is tractable for different type of nonlinearity, to compute the nonlinear quantum modes. In the present paper, our previous developments are used to evaluate the coherent dynamical structure factor (DSF) of the KG lattice, at low temperature. The contribution to the DSF of the nonlinear quantum modes, known as either the phonon bound states[6,7,21,22,28] or else the quantum breathers,[11,14–16,20] is the central purpose of our work. As the DSF standard derivation is obtained in the harmonic approximation,[1,4] treating the anharmonicity as a perturbation, we propose a different scheme where this approximation is not required. For instance, the Bloch identity, which is a key for the conventional calculation, is not invoked in our theory. We simply introduce a Taylor expansion of the DSF with respect to the atomic displacements, computing numerically the coefficients of the series. Our method

is tested by comparison to the standard analytical calculation on the purely harmonic lattice. Our approach allows us to deal with different strength of the anharmonicity. When the on-site nonlinearity dominates the intersite coupling, the nonlinear quantum modes lead to some anharmonic resonances well separated from the multiphonon continua, in the inelastic spectrum. These anharmonic resonances have the same order as for the fundamental phonons whereas the unbound multiphonons yield a DSF at least one order below. On the other hand, their dispersion is found to decrease dramatically with the value of the energy transfer, which differentiates them from the broad phonon resonance. By way of contrast, when the intersite coupling is larger than the on-site nonlinearity, the anharmonicity of the spectrum is weak compared to the phonon dispersion. In such a quasiharmonic lattice, the dynamical response of the biphonon (a two-phonon bound state) may yet exhibit a significant magnitude, still much larger than the two phonon, even though the biphonon resonance occurs at an energy transfer that approaches the unbound phonons band. Actually, the biphonon signature is found to dominate the two-phonon DSF provided that the lattice nonlinearity is not strictly zero. Alongside our numerics, a perturbation theory is developed and proves accurate for strongly nonlinear lattices. We also show how the model parameters may be adjusted so as to work out the energy landscape of the inner particles as well as their interactions. Finally, the present study will serve as a basis for future simulations of the KG incoherent scattering cross section.

After a brief introduction to the nonlinear KG lattice, the DSF is derived in Sec. II. In Sec. III, our results are detailed and commented while the Sec. IV summarizes them and draws some perspectives.

II. COHERENT DYNAMICAL STRUCTURE FACTOR OF THE NONLINEAR KG LATTICE

We assume that some light particles form a regular network, whether it is inside a molecule or a crystalline solid. Were the particle dynamics independent, the Hamiltonian would have read

$$H_0 = \sum_l \left[\frac{p_l^2}{2m} + V(x_l) \right], \tag{1}$$

where x_l and p_l are displacement and conjugate momentum (i.e., $[x_l, p_l] = \hbar i$) of a particle at site l. For sake of simplicity,

we choose to work on a one-dimensional lattice with a single direction for the motion of atoms, denoted by the unit vector **u**, which is named as polarization in the followings. The single dimension proved relevant in several concrete studies.[25,29] The local potential $V(x_l)$ may then be expanded as a fourth order series: $V(x_l) = a_2 x_l^2 + a_3 x_l^3 + a_4 x_l^4$. Some higher order terms could be added with no difficulties for our numerics, so as to simulate eventually a specific shape of V. In truth, the interaction between nearest neighbors, that may be direct or mediated by the heavy atoms that compose the skeleton of a material, involves a displacement coupling that is modeled by a quadratic term. So the Hamiltonian of the particle ensemble now reads

$$H = H_0 - c \sum_{l,j=\langle l \rangle} (x_l - x_j)^2, \qquad (2)$$

where c is the coupling parameter and the symbol $(\langle l \rangle)$ describes the first neighbors of the site labeled by l. Introducing the dimensionless operators P_l and X_l, the Hamiltonian can be reformulated as follows:

$$H = \hbar \Omega \sum_l \left[\frac{P_l^2}{2} + A_2 X_l^2 + A_3 X_l^3 + A_4 X_l^4 + \frac{C}{2} X_l \sum_{j=\langle l \rangle} X_j \right], \qquad (3)$$

where the fundamental frequency Ω, as well as the dimensionless coefficients A_3, A_4, and C have been defined in Ref. 32. The total number of sites is denoted by N, the lattice parameter by a_0 and the orientation of the chain is defined by a unit vector **v**. We introduce ψ, the eigenstates of H, and particularly the ground state ψ_{GS}, the phonons $\psi_{ph}(\mathbf{k})$ and the biphonons $\psi_{bi}(\mathbf{k})$. These states are computed numerically[32] as well as their eigenvalues E_{GS}, $E_{ph}(\mathbf{k})$, and $E_{bi}(\mathbf{k})$, respectively. The wave momentum, denoted by **k**, verifies $\mathbf{k} = (2\pi k/Na_0)\mathbf{v}$ where k is an integer. The ground state wave momentum $\mathbf{k}_0$ takes its value in the reciprocal lattice, $\mathbf{k}_0 = (2\pi k_0/a_0)\mathbf{v}$ where k_0 is an integer. Apart when it will be noted, k_0 is fixed to zero. The lattice is assumed to be maintained at very low temperature, i.e., $kT < E_{ph}$, so the scattering induces some excitations solely from ψ_{GS}. The transition probability is proportional to the DSF:[4]

$$S(\mathbf{q}, \omega_{\psi(\mathbf{k})}) = \frac{1}{N} \left| \sum_j \langle \psi_{GS} | e^{i[\mathbf{q} \cdot \mathbf{r}_j]} | \psi(\mathbf{k}) \rangle \right|^2, \qquad (4)$$

where $\omega_{\psi(\mathbf{k})} = (E_{\psi(\mathbf{k})} - E_{\psi_{GS}})/\hbar$, **q** is the scattering vector and $\mathbf{r}_j$ represents the atomic position at site j. That position can be expressed as $\mathbf{r}_j = ja_0\mathbf{v} + \mathcal{L}X_j\mathbf{u}$, where $\mathcal{L} = \sqrt{\hbar/(m\Omega)}$ is the length scale of vibrations, fixed to a reasonable value of 3% of a_0. The polarization vector **u** is the principal axis of atomic displacement around the equilibrium position $(ja_0\mathbf{v})$. We now spell out our method for computing the DSF. As, strictly speaking the Bloch identity does not hold for a nonlinear lattice,[4] we propose a derivation which differs from the conventional one. Since $\mathcal{L}$ is much smaller than a_0, the exponential function in Eq. (4) can be expanded as a Taylor series with respect to the weakest of its arguments, the term proportional to $\mathcal{L}$:

$$S(\mathbf{q}, \omega_{\psi(\mathbf{k})})$$

$$= \frac{1}{N} \left| \sum_j e^{i[\mathbf{q} \cdot \mathbf{v}]ja_0} \right.$$

$$\left. \times \sum_p \frac{(i[\mathbf{q} \cdot \mathbf{u}]\mathcal{L})^p}{p!} \langle \psi_{GS} | X_j^p | \psi(\mathbf{k}) \rangle \right|^2. \qquad (5)$$

This development holds provided that the order of the expansion is large enough. The series convergence has been tested by increasing the order up to reach the desired precision. The agreement to the standard analytical calculation on the purely harmonic lattice (see Sec. III) is a necessary condition of validity that has been fulfilled too. In the left hand side of Eq. (5), the bracket $\langle \psi_{GS} | X_j^p | \psi(\mathbf{k}) \rangle$ can be replaced by $\langle \psi_{GS} | X_0^p | \psi(\mathbf{k}) \rangle$ multiplied by a phase factor $e^{-i([\mathbf{k} \cdot \mathbf{v}]a_0 j)}$, because of the translational invariance. The sum over the subscript j in Eq. (5) gives zero for all **q**, aside from the wave vectors that match the momentum conservation $[(\mathbf{q} - \mathbf{k}) \cdot \mathbf{v}] = 0$. This condition, as well as the conservation of the energy are supposed to be satisfied for a given state $\psi(\mathbf{k})$. The calculation of $S(\mathbf{q}, \omega_\psi)$ can then be reduced to the determination of the bracket $D[\psi(\mathbf{k}), p] = \langle \psi_{GS} | X_0^p | \psi(\mathbf{k}) \rangle$, since one may check that

$$S(q, \omega_{\psi(\mathbf{k})}) = N\delta_{[(\mathbf{q} - \mathbf{k}) \cdot \mathbf{v}]} \left| \sum_p \frac{(i[\mathbf{q} \cdot \mathbf{u}]\mathcal{L})^p}{p!} D[\psi(\mathbf{k}), p] \right|^2. \qquad (6)$$

We study the variation of the DSF along a single direction which the angles with respect to **u** and **v** are α_u and α_v, respectively. Then $S(\mathbf{q}, \omega_\psi)$ depends only on the magnitude of the momentum transfer $|\mathbf{q}|$ along that direction and the conservation law fixes $|\mathbf{q}|\cos(\alpha_v) = [\mathbf{k} \cdot \mathbf{v}]$. This condition can be achieved whether $|\alpha_v| \neq \pi/2$ which may be reasonably assumed for a low-angle scattering. In a same manner, when $|\alpha_u| = \pi/2$ the inelastic part of the structure factor is identically null because $[\mathbf{q} \cdot \mathbf{u}] = 0$ (excepted for the elastic DSF which then equals N). Consequently, we assume that $|\alpha_v| = |\alpha_u| \neq \pi/2$ which keeps the physics of our problem, avoiding the unimportant cases. We denote by q the scalar product $[\mathbf{q} \cdot \mathbf{u}]$ for a vector **q** that matches the conservation law, so that we have also $q = [\mathbf{k} \cdot \mathbf{v}]$. Then, the DSF reads

$$S(q, \omega_{\psi(q)}) = N \left| \sum_p \frac{(iq\mathcal{L})^p}{p!} D[\psi(q), p] \right|^2. \qquad (7)$$

Since the optical modes are characterized by a weak value of C in Eq. (3), the first step of our treatment is concerned with a perturbation theory with respect to the intersite coupling. At $C = 0$, namely the anti-continuum (e.g., uncoupled, atomic or molecular) limit,[10] the phonon states and the phonon bound states can all be written as some Bloch waves[32]

$$B_\alpha(\mathbf{k}) = \frac{1}{\sqrt{N}} \sum_j e^{-i[\mathbf{k} \cdot \mathbf{v}]a_0 j} \times \phi_{\alpha,j} \Pi_{l \neq j} \phi_{0,l}, \tag{8}$$

where $\phi_{\alpha,j}$ is an on-site wave function that depends only on X_j. Actually, $\phi_{\alpha,j}$ is the αth eigenstate of the on-site Hamiltonian

$$h_l = \frac{P_l^2}{2} + A_2 X_l^2 + A_3 X_l^3 + A_4 X_l^4. \tag{9}$$

To a first order in C, the lattice ground state ψ_{GS} is simply given by the product $B_0 = \Pi_l \phi_{0,l}$ while Eq. (8) gives a phonon for $\alpha = 1$ and a biphonon for $\alpha = 2$. Let us denote by $V_{\alpha,n}$, the projection of the state ϕ_α onto the nth on-site harmonic os-

cillator eigenstate $|n\rangle$ and develop the bracket $G(\alpha, 0, p) = \langle \phi_0 | X^p | \phi_\alpha \rangle$:

$$G(\alpha, 0, p) = \sum_{n \geq 0, m \geq 0} V_{0,m} V_{\alpha,n} \langle m | X^p | n \rangle, \tag{10}$$

where the subscript has been dropped for ease. We point out that for $C = 0$, we have $D[B_\alpha(\mathbf{k}), p] = G(\alpha, 0, p)/\sqrt{N}$ and $D(B_0, p) = G(0, 0, p)$. One more thing has to be done before reaching our goal, is to compute $\langle m | X^p | n \rangle$. To that purpose, the Bose-Einstein operators [i.e., $a^+ = \sqrt{2}(X - iP)$ and $a = \sqrt{2}(X + iP)$] are used to expand X^p. We wrote a Fortran program which realizes the expansion, respecting the commutation rule, $[a, a^+] = 1$. For example, the output for $p = 10$ is

$$X^{10} = \frac{1}{32}[a^{+10} + a^{10} + 10(a^+ a^9 + a^{+9} a) + 45(a^{+2} a^8 + a^{+8} a^2 + a^{+8} + a^8) + 120(a^{+3} a^7 + a^{+7} a^3) + 360(a^+ a^7 + a^{+7} a) + 210(a^{+4} a^6$$
$$+ a^{+6} a^4) + 1260(a^{+2} a^6 + a^{+6} a^2) + 630(a^{+6} + a^6) + 252 a^{+5} a^5 + 2520(a^{+5} a^3 + a^{+3} a^5) + 3780(a^{+5} a + a^+ a^5) + 3150(a^{+4} + a^4$$
$$+ a^{+4} a^4) + 4725(2 a^{+2} a^4 + 2 a^{+4} a^2 + 4 a^{+2} a^2 + a^{+2} + a^2 + 2 a^+ a) + 12600(a^+ a^3 + a^{+3} a + a^{+3} a^3) + 945]. \tag{11}$$

The writing of X^p would take more than one full page for values of p larger than 30. Our program allows us to compute the bracket $\langle m | X^p | n \rangle$ up to the power $p = 60$, for different integers m and n. The association of this program with the numerical diagonalization of h_l [Eq. (9)] which fixes the coefficients $V_{\alpha,n}$ in Eq. (10),[32] permits us to compute the coefficients $G(\alpha, 0, p)$ that can be tabulated for different model parameters. Finally, to a first order in C, one obtains

$$S(q, \omega_{B_\alpha(q)}) = \left| \sum_p \frac{(iq\mathcal{L})^p}{p!} G(\alpha, 0, p) \right|^2 \tag{12}$$

for the inelastic scattering where the momentum conservation imposes $q = 2\pi k/(Na_0)$, whereas the elastic response is given by

$$S(q, 0) = N \left| \sum_p \frac{(iq\mathcal{L})^p}{p!} G(0, 0, p) \right|^2, \tag{13}$$

where $q = 2\pi k_0/a_0$ [k and k_0 range over integers]. Formally, these results are given for a one-dimensional lattice but they can be extended to higher dimensional lattice by summing over the coordinates and polarizations. To a first order in C, the frequency $\omega_{B_\alpha(q)}$ can also be evaluated by

$$\omega_{B_\alpha(q)} = \Omega[\gamma_\alpha - \gamma_0 - 2C \times G(\alpha, 0, 1)^2 \cos(qa_0)], \tag{14}$$

where the coefficient γ_α is the eigenenergy of h_l [Eq. (9)] associated to Φ_α. For the perfect harmonic lattice, the first order in C in the standard calculation[1,4] of $S(q, \omega)$ is equivalent to Eqs. (12) and (13).

When C is large, the Hamiltonian in Eq. (3) must be diagonalized numerically after expanding in a suitable basis. We worked with a Bloch wave basis[32] given by

$$B_{[\Pi_j \alpha_j]}(\mathbf{k}) = \frac{1}{\sqrt{A_{[\Pi_j \alpha_j]}}} \sum_j e^{-i[\mathbf{k} \cdot \mathbf{v}]a_0 j} \times \Pi_l \phi_{\alpha_l, l+j}, \tag{15}$$

where $A_{[\Pi_j \alpha_j]}$ ensures the normalization. Each eigenstate, characterized by a wave vector $\mathbf{k}$, can be written as a linear combination of those Bloch waves

$$\psi(\mathbf{k}) = \sum_{\Pi_j \alpha_j} W_{\psi, \Pi_j \alpha_j} B_{[\Pi_j \alpha_j]}(\mathbf{k}), \tag{16}$$

where the subscript $\Pi_j \alpha_j$ identifies a single Bloch wave in Eq. (15). The numerical diagonalization has been carried out for different lattice sizes with no noticeable discrepancy in the eigenspectrum in increasing N. In Fig. 1, the same energy cutoff on the Bloch wave basis has been fixed for both $N = 23$ and $N = 33$. Apart on their wave vector, the eigenvalues are found to be independent of N. In Fig. 1(a), the optical phonon branch is plotted whereas, in Fig. 1(b), the energy region of the first overtone is plotted for same parameters as in (a). One notes clearly the biphonon branch and the two-phonon band, thoroughly described elsewhere.[7,17,20,32,33] Interestingly, for small enough nonlinear parameters, the anharmonicity of the lattice is negligible compared to the phonon branch width and the biphonon branch disappears [see Fig. 1(c)]. The bracket $D(\psi, p)$ can now be written as follows:

$$D[\psi(\mathbf{k}), p]$$
$$= \sum_{(\Pi_j \alpha_j, \Pi_j \beta_j)} W^*_{\psi_{GS}, \Pi_j \beta_j} W_{\psi, \Pi_j \alpha_j} \langle B_{[\Pi_j \beta_j]}(0) | X_0^p | B_{[\Pi_j \alpha_j]}$$
$$\times (\mathbf{k}) \rangle, \tag{17}$$

where the last term in the right hand side can be detailed further
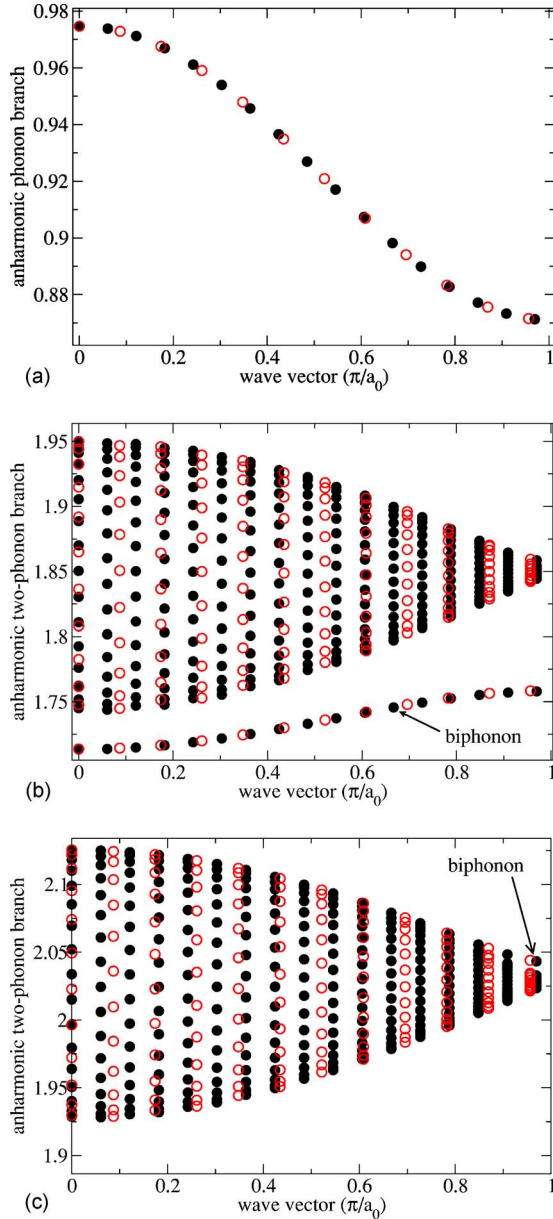
FIG. 1. (Color online) energy spectrum of a chain composed of N unit cells, $N=33$ (full circles) and $N=23$ (empty circles): (a) the optical phonon branch for model parameters $C=0.05$, $A_3=0.12$ and $A_4=0.01$; (b) the two-phonon energy region for the same parameters as (a); (c) the same as in (b) but for $C=0.05$, $A_3=0.05$ and $A_4=0.01$. The Y axis unit is $\hbar\Omega$. The wave vector is reported on the X axis, whose unit is (π/a_0) and ranges over the lattice first Brillouin zone.

$$\langle B_{[\Pi_j\beta_j]}(0)|X_0^p|B_{[\Pi_j\alpha_j]}(\mathbf{k})\rangle = \frac{1}{\sqrt{A_{[\Pi_j\alpha_j]}A_{[\Pi_j\beta_j]}}}\sum_{n_1,n_2} e^{-i[\mathbf{k}\cdot\mathbf{v}].a_0 n_1}$$
$$\times \Pi_{l\neq j}\delta(\alpha_{l+n_1},\beta_{l+n_2})G$$
$$\times (\alpha_{l+n_2},\alpha_{l+n_1},p). \qquad (18)$$

This equation concludes our computation task on the KG lattice dynamical response to the scattering of a external beam of light or particles. Our numerical treatment, includ-

ing the diagonalization of H and the computations of Eqs. (7), (17), and (18) takes few hours on a conventional desktop PC. The convergence of the series in Eq. (7) has been tested by comparing our results for different development orders, e.g., 30, 40, 50, and 60. As expected, the smaller is the scattering vector, the better is the precision. For a momentum transfer that ranges over 30 lattice Brillouin zones, the difference between the DSF computed with series orders 50 and 60 is less than 1%.

III. RESULTS AND DISCUSSIONS

Figure 2 shows our typical result that is a three-dimensional (3D) plot of the inelastic $S(q,\omega)$ for a nonlinear lattice whose model parameters are those of Figs. 1(a) and 1(b). Three noteworthy resonances emerge with same order of magnitude. These three resonances correspond to the eigenenergies of the nonlinear phonon states, i.e., the phonons, biphonons, and triphonons. The binding energy of the biphonon, evaluated at the center of the Brillouin zone (BZ) is around a few percent of the fundamental phonon excitation. Several model parameters have been tested and lead to qualitatively similar results. For instance, besides the different values of the energy transfer, the biphonon and triphonon resonances occur in a lattice with a quadratic-quartic on-site potential, i.e., $A_3=0$ in Eq. (3). In the biphonon and triphonon resonances, one may recognize some peaks that will be examined further. In order to analyze our results more quantitatively it is, though, easier to work with a two-dimensional (2D) plot that represents the $S(q,\omega)$ profile versus the projection $q=[\mathbf{q}\cdot\mathbf{u}]$ of the scattering vector $\mathbf{q}$. In order to verify the accuracy of our computations, presented in Sec. II, we compare our numerical results to the exact analytical ones that are achieved in a purely harmonic lattice. In that case, the profile of the Debye-Waller factor, i.e., $S(q,0)/N$ is plotted in Fig. 3 and shows a convincing agreement since our numerical results scarcely differ from the analytical ones. It ensures us that our series expansion of $S(q,\omega)$ has converged. Only the nonzero values of the Debye-Waller have been retained in the plot, i.e., $q=2\pi k_0/a_0$. A similar accord is obtained for the inelastic part of $S(q,\omega)$ (see further in the same section). The calculation made in a standard harmonic approximation[4] gives a Gaussian dependency of the Debye-Waller factor $S(q,0)/N = \exp[-2W(q)]$ where $2W(q)=(q\mathcal{L})^2|\langle\psi_{GS}|X_j^2|\psi_{GS}\rangle|$. In this expression, the bracket is simply given by $1/(2N)\Sigma_k 1/\omega_{ph}(K)$ where $\omega_{ph}(K)=\sqrt{1+2C\cos(K\cdot a_0)}$ and K ranges in the first BZ. When the nonlinear parameters are no longer negligible in Eq. (3), we note, in Fig. 3 that the Debye-Waller of a nonlinear lattice differs from the harmonic one. The Gaussian form is yet roughly conserved so there is no qualitative changes involved by the on-site anharmonicity. Our perturbation theory proves sufficient under the condition that the intermolecular coupling is not too large. In agreement with our results, the earlier study of Thompson[34] concluded that a cubic-anharmonic term involved a negligible correction upon the Debye-Waller factor. The calculation of Thompson is, in fact, a second order perturbation in
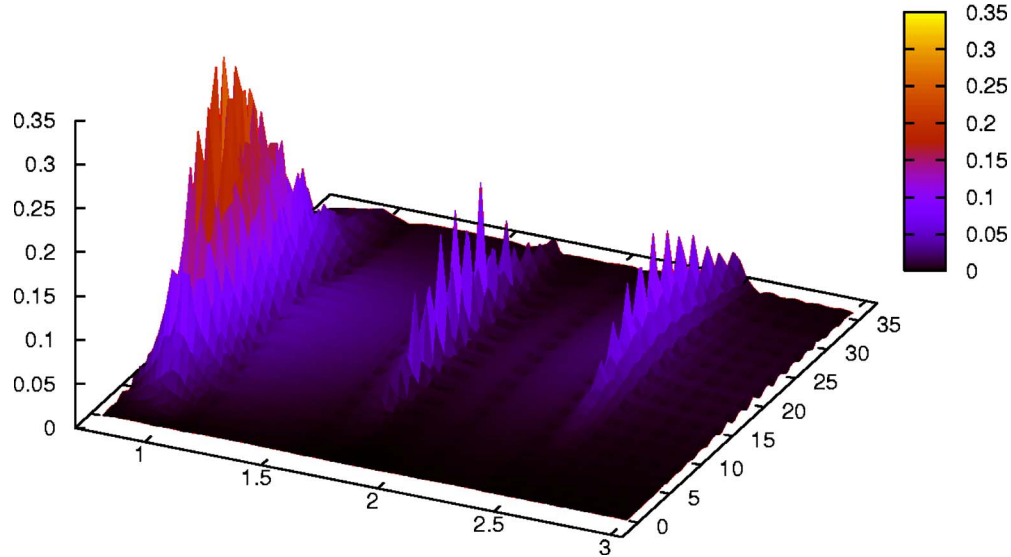
FIG. 2. (Color online) A 3D plot of the inelastic $S(q, \omega)$ as a function of the dimensionless energy transfer ω and the scalar product $q = [\mathbf{q} \cdot \mathbf{u}]$ of the transfer momentum $\mathbf{q}$ and the polarization $\mathbf{u}$. The parameters are the same as in Figs. 1(a) and 1(b). The figure is easier to depict in color.

the cubic term, which is thus assumed to be weak enough for the perturbation theory to be valid. Not surprisingly, it leads to a correction that is also weak. However, as we shall see, the most significant contribution of the nonlinearity to the DSF spectra proves to be inelastic and is due to the phonon bound states.

In a same manner as for the elastic scattering, our numerical computation of the inelastic DSF is compared to the exact calculation[4] in the case of a harmonic lattice. The contribution of phonon states is then given by

$$S[q, \omega_{ph}(q)] = \frac{q^2}{2\omega_{ph}(q)} \exp[-2W(q)], \qquad (19)$$

with same notations as previously used in the same section. The obtained agreement, demonstrated in Fig. 4, confirms the validity of our theoretical approach and consequently the convergence of our series development. The DSF profile appears as being continuous because the lattice size is large enough to blur the discreteness of the Fourier space at the scale of Fig. 4, which ranges over 60 BZ. Apart from the $S(q, \omega)$ ripple, the perturbation theory captures quite well the main variations of the envelope of $S(q, \omega_{ph})$. This ripple stems from the dispersion of ω_{ph} and so, its amplitude in-
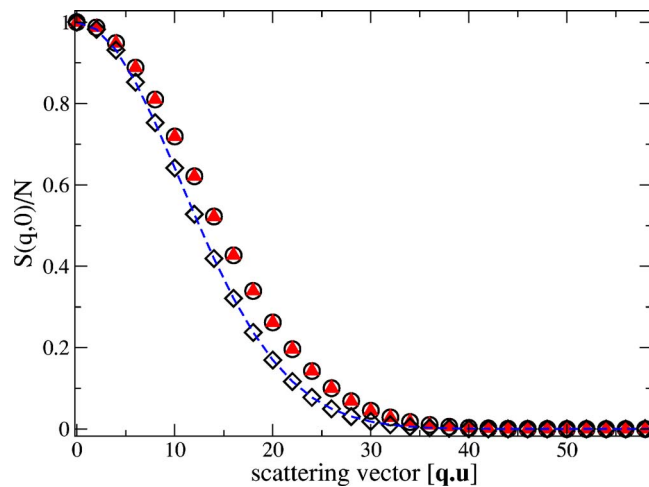

FIG. 3. (Color online) A plot of the Debye-Waller factor $[S(q, \omega=0)/N]$ vs the scalar product $q = [\mathbf{q} \cdot \mathbf{u}]$, for different model parameters. Each symbol corresponds to a Bragg peak. Our numerical results are reported for $C = 0.05$, $A_3 = A_4 = 0$ (diamonds), and $C = 0.05$, $A_3 = 0$, $A_4 = 0.2$ (triangles). The exact formula derived in a harmonic model (dashed line) confirms the former while the latter has been computed within a perturbation theory (circles) too. The X axis, which unit is π/a_0 bears the scattering vector q over a range of 60 Brillouin zones.
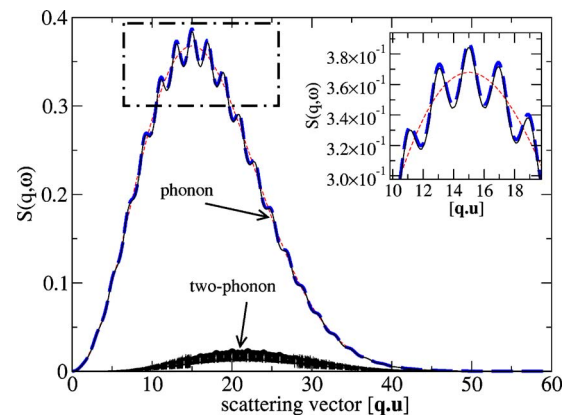

FIG. 4. (Color online) A plot of the coherent inelastic $S(q, \omega)$ profile versus $q = [\mathbf{q} \cdot \mathbf{u}]$, for phonon in a harmonic lattice: $C = 0.05$, $A_3 = A_4 = 0$. The thin dashed line has been obtained by a perturbation theory. The thin solid line corresponds to our numerical treatment and the thick dashed line to a plot of the exact formula (see Ref. 4) (the two latest curves are hardly distinguished in the graph). In the inset, the area in the dot-dashed rectangle is magnified. The X axis unit is π/a_0.
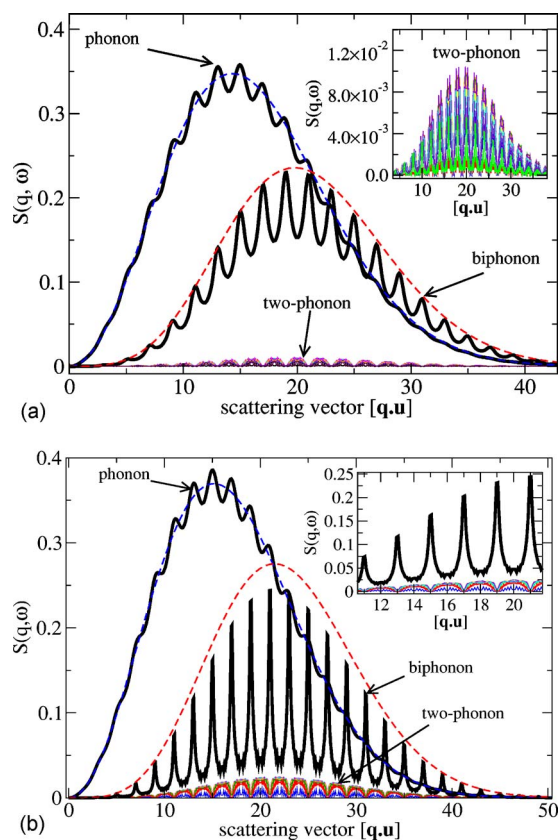
FIG. 5. (Color online) A plot of the coherent inelastic $S(q,\omega)$ profile versus $q=[\mathbf{q}\cdot\mathbf{u}]$, for phonon, biphonon, and two-phonon states. The model parameters are: (a) $C=0.05$, $A_3=0.12$, and $A_4=0.01$; (b) $C=0.05$, $A_3=0.05$, and $A_4=0.01$. The dashed lines correspond to our perturbation theory and the solid lines to our numerical treatment. The X axis unit is π/a_0 and the scattering vector q ranges over 60 Brillouin zones. The inset shows a magnification of the two-phonon contributions.

creases with C to become some peaks for the acoustic phonons in a harmonic lattice.[36] When the sign of C is inverted in our model (C becomes negative), the local minima of $S(q,\omega_{ph})$ are shifted at the edges of the lattice Brillouin zones instead of being in the middle when $C>0$. In Fig. 4, the DSF resonance involved by the two-phonon states is also plotted. It is usually termed multiple scattering and is one order of magnitude smaller than the one-phonon process. If the anharmonicity of V cannot be neglected, the profile of the one-phonon resonance in $S(q,\omega)$ shows no qualitative changes compared to the harmonic lattice [see Figs. 4 and 5(a)]. However, the response of the biphonon, whose profile is denoted by $S(q,\omega_{bi})$, appears clearly at higher energy transfer than one phonon [see Figs. 2 and 5(a)]. The resonance associated to the biphonon is one order of magnitude larger than for the unbound phonon states and has same order as $S(q,\omega_{ph})$. A gap is opened between the biphonon branch and the two-phonon band [Fig. 1(b)] so the biphonon resonance occurs for an energy transfer which does not match the harmonics of the fundamental phonons. As mentioned above, that energy gap is also called the binding energy of the biphonon.[7] It is also worth noting that the maximum of the $S(q,\omega_{bi})$ envelope is reached for a scattering vector that dif-

fers from the envelope maximum of $S(q,\omega_{ph})$. This maximum occurs, indeed, at larger q for the biphonon. The $S(q,\omega_{bi})$ envelop can be evaluated within the perturbation theory [see Figs. 5(a)] which provides a rather satisfactory approximation, although the $S(q,\omega_{bi})$ ripple has a larger amplitude than for phonons. To interpret our results, it is needed to dwell on the ripple of the biphonon contribution to the DSF. As for the phonon, this ripple is related to the dispersion of the biphonon branch. In the case where the binding energy of biphonon is not very large, say no more than a few percent of the phonon energy, the different bottoms of the $S(q,\omega_{bi})$ ripple occur at center of the successive BZ while the tops are reached at the BZ edges. According to several tests, it is a systematic feature which, in contrast to phonon, does not depend on the sign of C. Moreover, as shown in the insets of Figs. 5(a) and 5(b), the minima of $S(q,\omega_{bi})$ and the maxima of the two-phonon resonance correspond one to one. That may be explained as follows. In our perturbation theory the biphonon states are approximated by the Bloch waves that bear a single on-site excitation, $\alpha=2$ in Eq. (8). In case $C\neq 0$, since the biphonon binding energy is not very large, these Bloch waves are hybridized with some other Bloch waves, given by Eq. (15), and particularly those bearing two on-site excitations $\alpha=1$, at different sites. The degeneracy lifting of the latest states yields the unbound two-phonon band. The ripple of the DSF cannot be analyzed through our first order perturbation theory [see Figs. 5(a) and 5(b)], which hints that it is due to the Bloch waves hybridization, involved by the intersite coupling. The discrepancy of the perturbation theory Eq. (12) increases as the biphonon gap decreases [compare Figs. 1(b) and 1(c) to Figs. 5(a) and 5(b)] because of the hybridization step-up. The gap between the biphonon branch and the unbound two-phonon band is smaller at the center of each BZ [see Fig. 1(b) and Ref. 32] because here the width of the two-phonon band is maximum. The smaller the energy gap is the larger the hybridization is, so as a result, one finds a larger contribution of the two on-site excitation Bloch waves into the biphonon eigenstate at the center of each BZ. The Bloch waves with multiple excitations at distinct sites yield a zero response to scattering, $S(q,\omega)=0$. One deduces that the biphonon response $S(q,\omega_{bi})$ is minimum when the contribution of the two on-site excitation Bloch waves is maximum, i.e., at the center of each BZ. On the other hand, the unbound two phonons resonance comes to a maximum at the center of each BZ because of the contribution of the Bloch waves with a single on-site excitation $\alpha=2$ to the two-phonon eigenstates. Conversely, at the edge of the lattice Brillouin zones, the Bloch wave hybridization is minimum (because the energy gap is maximum) so that the biphonon response is maximum and may even reach the value computed within the perturbation theory [Fig. 5(b)]. Another interesting point that is made clear within the previous discussion is why the $S(q,\omega_{bi})$ ripple is not shifted when the sign of C is changed, unlike $S(q,\omega_{ph})$. Indeed, reversing the C sign leaves unchanged the two-phonon band shape, i.e., the band width is still maximum at the BZ center. So it is for the biphonon branch which the dispersion is mainly due to the contribution of the two on-site excitation Bloch waves[32] [the dispersion computed

within Eq. (14) for $\alpha=2$ is much smaller than the effective biphonon bandwidth]. So the gap between the biphonon and two-phonon bands is equally unchanged under the inversion of the coupling sign, i.e., the energy gap is still maximum at the BZ edges and minimum at the center. According to our analysis of the $S(q,\omega_{bi})$ ripple, it makes clear why the maxima and minima of the biphonon DSF are independent of the sign of C. Our argumentation holds provided that the biphonon binding energy remains inferior to a few percent of the fundamental excitations.

When the anharmonicity of V is weak compared to the phonon bandwidth, the biphonon gap closes and a pseudogap forms[35] at the edge of the lattice Brillouin zones. Then the biphonon branch hardly appears nearby the two-phonon band [see Fig. 1(c)]. The lattice is said quasiharmonic since the spectrum anharmonicity vanishes. There is, indeed, no anharmonic resonances, neither in the density of state nor, accordingly, in the DSF. That may happen for higher order phonon bound states as the hardening of the quartic on-site term in V [Eq. (3)] could compensate the softening of the cubic potential in a certain range of energy, although that seemingly perfect harmonicity, the $S(q,\omega)$ ripple may yet betray the nonlinearity of V. In truth, at the BZ center, the DSF associated to the biphonon, referred to as $S(q,\omega_{bi})$, has same order as the DSF of two-phonon states, whose magnitude is one order below the phonon resonance [see Fig. 5(b)]. In contrast, the profile $S(q,\omega_{bi})$ reaches its maxima where the pseudogap opens [see Fig. 1(c)], i.e., at the BZ boundaries and the ripple alongside each BZ can be seen as a series of peaks. In Fig. 5(b), the largest peak remains much larger than the two-phonon response and it has same order as the maximum of the phonon DSF profile, $S(q,\omega_{ph})$. The maxima of the biphonon DSF decrease as the nonlinear parameters tend to zero. However, before reaching that point, we have seen that the anharmonicity of the energy spectrum vanishes as in Fig. 1(c). Consequently, we propose to dub the $S(q,\omega_{bi})$ peaks by nonlinear Bragg peaks, since they gather two features that are opposite to the usual Bragg scattering: first, they are inelastic peaks and second, they satisfy the Bragg reflection condition but shifted of a half reciprocal lattice vector (i.e., π/a_0 for the one-dimensional chain). According to Ref. 35, the pseudogap may occur in lattices with a higher dimension so that similar results as those presented here can be expected in different lattices. In spite of the relative simplicity of our model compared to the case encountered in practice, it indicates that the biphonon may still emerge and contribute significantly to the scattering, even though the spectrum seems perfectly harmonic. In Figs. 1(c) and 5(b), we have chosen intentionally a set of parameters that yields a eigenspectrum which is almost harmonic. A pseudogap hardly opens between the biphonon branch and the two-phonon band. The parameter A_3 could be doubled [as in Fig. 2(c) in Ref. 35] without opening a substantial gap which would permit one to identify the anharmonicity in the energy density of state. In fact, the larger is the phonon dispersion the larger is the range of nonlinear parameters that leads to a quasiharmonicity. In Fig. 6(a) the profile of $S(q,\omega)$ is plotted for different values of the energy transfer ω, e.g., ω_{ph} for phonon, ω_{bi} for biphonon and ω_{tri} for triphonon. The triph-
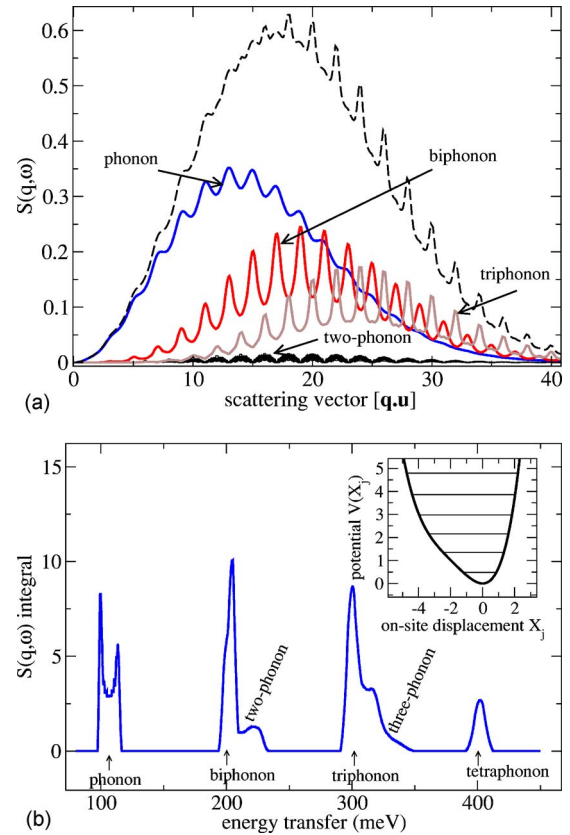

FIG. 6. (Color online) In (a), the same as in Fig. 5(a) but for different model parameters: $C=0.06$, $A_3=0.17$, and $A_4=0.0231$. In addition, have been plotted the $S(q,\omega)$ profile for the triphonon and the integral of $S(q,\omega)$ over the energy transfer ω (dashed line). The elastic contribution has been skipped. In (b), a plot of the profile of the $S(q,\omega)$ integral over the reciprocal lattice (see text), vs the energy transfer ω, for same parameters as in (a). The inset in (b) shows the corresponding potential landscape $V(X_j)$ and its quantum levels. Our energy unit $\hbar\Omega$ has been fixed to 107 meV.

onon resonance is found to reach a significant magnitude that is comparable to phonon and biphonon. Such a high order phonon bound state has been identified in different materials, e.g., TiH,[28] ZrH,[29] and HCl.[22] It is worth noting the triphonon spectrum ripple, which originates from the hybridization between the bound and unbound phonon states, as for the biphonon spectrum. This triphonon ripple is shifted of π/a_0 compared to the biphonon DSF profile.

If one assumes that the energy resolution is not sufficient to differentiate the inelastic lattice resonances (as it may be the case, for instance, in the inelastic x-ray scattering), we have to integrate our simulation with respect to the energy transfer ω. The elastic contribution is skipped from that integral so as to distinguish the inelastic part of the DSF. We computed the corresponding integral and reported the result as a dashed line in Fig. 6(a). The amplitude and the position of the maximum of the DSF integral are related to the nonlinear parameters. In a strictly harmonic lattice, that integral scarcely differs from the phonon response, whereas in Fig. 6(a) we note a clear difference between the dashed line and the profile $S(q,\omega_{ph})$. The of the DSF integral has a form that might be fitted by a superposition of two Gaussian functions,

centered at different momenta. It is a standard treatment in the interpretation of the experimental $S(q,\omega)$ profile. If the nonlinear Bragg peaks are large (i.e., when the anharmonicity is weak compared to the phonon dispersion but that is yet not negligible) they may emerge in the integral as shown for large q in Fig. 6(a). In a strongly nonlinear lattice, a large gap separates the biphonon branch from the two-phonon energy band so the nonlinear Bragg peaks shrink to a ripple. Then it becomes rather difficult to depict the contribution of the nonlinear states in the DSF integral, aside from the shift of the envelop to larger **q**. On the other hand, if the energy resolution is sufficient to resolve the energy dispersion of the phonon branch but the accuracy over the scattering vector is not to separate the BZ (as it may be the case, for instance, in the neutron scattering of a powder specimen, since **u** and **v** are randomly distributed), then our calculation must account for superposition of the contributions of distinct BZ. As in a one-dimensional lattice the only symmetry is the inversion, we have to sum the factor $2S[q+k_0,\omega(q)]$ over the reciprocal vector k_0, where $q+k_0$ and $\omega(q)$ are both assumed to match the momentum and the energy conservation, respectively. Since $S[q+k_0,\omega(q)]$ decreases exponentially for a large enough value of $(q+k_0)$ [see Fig. 6(a)], the sum is ensured to be finite. Our energy resolution is assumed to be a triangle function centered at ω with a width of 0.02ω. The result of our treatment is shown in Fig. 6(b). We note the three resonances due to the nonlinear states, i.e., the biphonon, the triphonon and the quadriphonon that are separated from the broad resonances of either the phonon or the unbound phonons. It is noteworthy that the amplitude of the nonlinear resonances has same order as for phonons. Similar calculations with different model parameters even showed that, for a stronger anharmonicity the nonlinear resonances may be even larger in magnitude. The reason for such a behavior is that the density of state enhances as the eigenstates bandwidth decreases. This effect is sharp around the narrow branches as those of phonon bound states[38] [see Fig. 1(b)] which explains why the biphonon resonance may dominate the phonon one. The increase in the density of state may be recognized too in the single phonon response because the phonon branch is flat at the edge and at the center of the lattice BZ [see Fig. 1(a)]. Thus one sees two sidebands in the phonon resonance, at the upper and lower boundary in energy. The form of the lattice response around the first and the second overtone energy regions, in Fig. 6(b), is qualitatively similar either to the infrared adsorption spectra[6] in crystals as CO_2, N_2O, and OCS or to the Raman spectrum of H_2 solid.[23] Indeed the emergence of a sharp peak, associated to a biphonon (or to a bivibron[23]) occurs near a small hill-like resonance that is due to the unbound phonon states. In our simulation, a gradual variation of the model parameters so as to decrease the anharmonicity shows the same behavior as the pressure-induced bound-unbound transition, at 25 GPa in H_2 solid,[23] or at 34 GPa in D_2 solid.[39] Around that transition, the biphonon (or bivibron) peak broadens and decreases in magnitude. In our model, the pressure variation can be simulated by a change of the coupling parameter C due to the fact that neighboring molecules are moved closer together because of the external pressure.

As we did not find in the literature any experiments that could be related precisely to our previous calculations, we enhance that whether the inelastic scattering is coherent or incoherent, the lattice resonances occur at same energy transfer. Thus, it is possible to adjust our model parameters so as to obtain resonances at same energy as experiments on incoherent INS. To illustrate that possibility in Fig. 6(b), we have chosen the case of metal hydrides shown in Fig. 2 of Ref. 37 where the phonon, biphonon, and triphonon resonances were clearly identified. Since we are studying the coherent DSF, an accurate simulation of the spectra obtained by Kolesnikov *et al.* for the incoherent INS is out of purpose. The amplitudes and widths of various resonances cannot be simulated. Moreover, we have currently no means to simulate the features of the analyzer. Our parameters adjustment in Fig. 6(b) has been carried out with an energy unit $\hbar\Omega\approx 107$ meV, a dimensionless coupling $C=0.06$ and the nonlinear parameters $A_3=0.17$ and $A_4=0.0231$. In that manner, the on-site nonlinearity and thus the energy landscape of the light particles, here the deuterium, may be worked out to a better accuracy than in a purely quadratic model [see the inset in Fig. 6(b)]. In their studies, Kolesnikov and co-workers[28,29,37] recognized the phonon bound states resonances in the INS spectra of TiH-D and ZrH-D. To analyze their experimental spectra, the authors compared their data to a simulation made with a one-dimensional boson Hubbard lattice. This model shows some similarities to the KG lattice as the single dimension and the anharmonicity which leads to phonon bound states. Thus, one may expect that a similar computation of the incoherent spectra could be possible.

Although our work is concerned with a one-dimensional lattice, the results of the present study should hold in higher dimension where the DSF depends on the lattice symmetries and polarizations. The extension to higher dimension could be achieved in our perturbation theory with no particular difficulty. This approach proves adequate under the condition that the intersite coupling is very weak. Our numerics, more accurate, could also be extended to higher dimension but that would require one either to use a powerful computer or else a dramatic restriction on the site number, which could yet be relevant for some molecules as benzene.[26]

IV. CONCLUSION

The DSF of the nonlinear KG chain has been calculated for different strength of the on-site anharmonicity. This has been possible thanks to our numerics that permit us to diagonalized accurately the nonquadratic Hamiltonian.[32] The DSF has been expanded as a Taylor series of the atomic displacements, which avoids the use of the conventional harmonic approximations. We found that the on-site nonlinearity leads to phonon bound states and consequently to some anharmonic resonances in the DSF spectrum, which somehow confirms other works on different quantum lattices.[18–20] The treatment of the intersite coupling in a perturbation theory proved satisfactory to tackle a lattice whose nonlinearity is stronger than the dispersion. In contrast, when the interaction between first neighbors dominates the on-site nonlinearity, which remains however nonzero, the amplitude of the dy-

namical structure factor makes visible the biphonon, although the energy transfer is almost harmonic. In such a case, the variation of the biphonon DSF with respect to the transfer momentum q exhibits some peaks that are much larger than the multiple scattering. This would hint that, provided that the DSF could be resolved accurately in q, the nonlinear behavior of certain materials could be worked out, even though their spectra show no apparent energy anharmonicity.

To approach some concrete cases, the theory requires further developments to consider, for instance, the three dimensionality of a realistic sample or the incoherent scattering. In a first step, this could be achieved within our perturbation theory. In addition to the possibility of simulating the incoherent INS in certain hydrides and molecular crystals, as those quoted in the present paper, it might be worth studying the nonlinear surface modes that could be investigated practically by different technics, e.g., electron scattering or infrared adsorption. The low dimensionality of the surface could give an advantage to achieve a simulation that would be physically accurate, particularly upon the lattice geometry and various polarizations. As an example, we note the case of the CO molecules adsorbed on a Ru(111) surface that has been studied both theoretically and experimentally.[40–42] As a low dimensional system, a vicinal surface, which might exhibit a regular one-dimensional nanostructure over several micrometers, would be the ideal substrate to explore the coherent scattering of appropriate nonlinear surface modes. The behavior of molecules adsorbed on a vicinal surface presents some specificity (see for instance Refs. 43 and 44, and references therein) and thus the feasibility of such a study remains under question, though, the aim would be to carry out a momentum resolved experiment, as those attempted on the PtCl ethylene diamine chlorate,[11,45] to check whether the predictions established within the KG model are confirmed in practice, especially about the biphonon contribution to the DSF. Another possibility to test our theory would be on the O_2 solid[11,46] where the oxygen cross section is mainly coherent. Although, in the β phase of the O_2 crystal, the intermolecular coupling overpasses the anharmonicity of the O_2 stretch,[46] our study showed that in such a case the inelastic scattering due to biphonon could yet be larger in magnitude than the two-phonon response. Further, the phonon bound states could emerge at higher energy transfer as found for the triphonon and quadriphonon in metal hydrides.[37] At least from a theory viewpoint, the β phase of the O_2 solid might be worth reexamining with recent experimental devices. Finally, according to the authors of Ref. 31, the potential landscape of hydrogen in PdH, that has been worked out from the INS spectra[31] agrees well with a first-principles calculation made independently.[47,48] On the basis of that successful comparison, one may expect that a standard first-principles theory could be used to calibrate the KG parameters so as to simulate *ab initio* the dynamical structure factor.

*Electronic address: lproville@cea.fr

[1] S. W. Lovesey, *Theory of Neutron Scattering from Condensed Matter* (Oxford Science, New York, 1984).

[2] E. Burkel, *Inelastic Scattering of X-Rays with Very High Energy Resolution* (Springer-Verlag, Berlin, 1991).

[3] M. De Crescenzi and M. N. Piancastelli, *Electron Scattering and Related Spectroscopies* (World Scientific, Singapore, 1996).

[4] N. W. Ashcroft and N. David Mermin, *Solid State Physics* (Saunders, Philadelphia, 1976), p. 790.

[5] N. W. Ashcroft and N. David Mermin, *Solid State Physics* (Saunders, Philadelphia, 1976), p. 487.

[6] F. Bogani, J. Phys. C **11**, 1283 (1978); **11**, 1297 (1978).

[7] V. M. Agranovich, *Spectroscopy and Excitation Dynamics of Condensed Molecular Systems* (North-Holland, New York, 1983), Chap. 3, pp. 83–138.

[8] A. J. Sievers and S. Takeno, Phys. Rev. Lett. **61**, 970 (1988); S. Takeno, K. Kisoda, and A. J. Sievers, Prog. Theor. Phys. Suppl. **94**, 242 (1988).

[9] R. S. MacKay and S. Aubry, Nonlinearity **7**, 1623 (1994).

[10] S. Aubry, Physica D **103**, 201 (1997).

[11] R. S. Mackay, Physica A **288**, 174 (2000).

[12] G. Kopidakis and S. Aubry, Phys. Rev. Lett. **84**, 3236 (2000).

[13] V. Hizhnyakov, D. Nevedrov, and A. J. Sievers, Physica B **316–317**, 132 (2002).

[14] J. Dorignac and S. Flach, Phys. Rev. B **65**, 214305 (2002).

[15] V. Fleurov, R. Schilling, and S. Flach, Phys. Rev. E **58**, 339 (1998).

[16] V. Fleurov, Chaos **13**, 676 (2003).

[17] J. C. Eilbeck, in *Localization and Energy Transfer in Nonlinear Systems*, edited by L. Vazquez, R. S. MacKay, and M. P. Zorzano (World Scientific, Singapore, 2003), p. 177.

[18] V. M. Agranovich and I. I. Lalov, Sov. Phys. Solid State **18**, 1148 (1976).

[19] O. A. Dubovskiĭ and A. V. Orlov, Phys. Solid State **40**, 670 (1998).

[20] W. Z. Wang, J. T. Gammel, A. R. Bishop, and M. I. Salkola, Phys. Rev. Lett. **76**, 3598 (1996).

[21] S. Califano, V. Schettino, and N. Neto, *Lattice Dynamics of Molecular Crystals* (Springer-Verlag, Berlin, 1981), pp. 215–259.

[22] C. Gellini, P. R. Salvi, and V. Schettino, J. Chem. Phys. **106**, 6942 (1997).

[23] H. Mao and R. J. Hemley, Rev. Mod. Phys. **66**, 671 (1994).

[24] B. I. Swanson, J. A. Brozik, S. P. Love, G. F. Strouse, A. P. Shreve, A. R. Bishop, W-Z. Wang, and M. I. Salkola, Phys. Rev.

Lett. **82**, 3288 (1999).

[25] F. Fillaux, B. Nicolaia, W. Paulus, E. Kaiser-Morris, and A. Cousson, Phys. Rev. B **68**, 224301 (2003).

[26] A. C. Scott and J. C. Eilbeck, Chem. Phys. Lett. **132**, 23 (1986).

[27] W. Jerzembeck, H. Bürger, V. Hänninen, and L. Halonen, J. Chem. Phys. **120**, 5650 (2004).

[28] A. I. Kolesnikov, M. Prager, J. Tomkinson, I. O. Bashkin, V. Yu Malyshev, and E. G. Ponyatovskii, J. Phys.: Condens. Matter **3**, 5927 (1991).

[29] A. I. Kolesnikov, I. O. Bashkin, A. V. Belushkin, E. G. Ponyatovskii, and M. Prager, J. Phys.: Condens. Matter **6**, 8989 (1994); I. O. Bashkin, A. I. Kolesnikov, and M. A. Adams, *ibid.* **12**, 4757 (2000).

[30] J. Eckert, J. A. Goldstone, D. Tonks, and D. Richter, Phys. Rev. B **27**, 1980 (1983).

[31] D. K. Ross, V. E. Antonov, E. L. Bokhenkov, A. I. Kolesnikov, E. G. Ponyatovsky, and J. Tomkinson, Phys. Rev. B **58**, 2591 (1998).

[32] L. Proville, Phys. Rev. B **71**, 104306 (2005).

[33] A. C. Scott, *Nonlinear Science* (Oxford, New York, 2003), Chap. 8, pp. 337–420.

[34] B. V. Thompson, Phys. Rev. **131**, 1420 (1963).

[35] L. Proville, Europhys. Lett. **69**, 763 (2005).

[36] In a harmonic lattice, the exact formula for $S(q,\omega)$ is given in the text of Sec. III and can be applied to the case of a linear KG lattice (strictly quadratic) with a large intersite coupling ($C=1/2$).

[37] A. I. Kolesnikov, A. M. Balagurov, I. O. Bashkin, A. V. Belushkin, E. G. Ponyatovsky, and M. Prager, J. Phys.: Condens. Matter **6**, 8977 (1994).

[38] A dispersionless branch corresponds to a Dirac function in the density of state.

[39] Jon H. Eggert, H.-K. Mao, and R. J. Hemley, Phys. Rev. Lett. **70**, 2301 (1993).

[40] P. Jakob and B. N. J. Persson, J. Chem. Phys. **109**, 8641 (1998).

[41] M. Bonn, C. Hess, and M. Wolf, J. Chem. Phys. **115**, 7725 (2001).

[42] V. Pouthier, J. Chem. Phys. **118**, 9364 (2003).

[43] M-C. Marinica and G. Raseev, Surf. Sci. **497**, 227 (2002).

[44] V. Pouthier and C. Girardet, Surf. Sci. **502/503**, 503 (2002).

[45] R. S. MacKay, ISIS Experimental Reports, RB10545 (2000).

[46] E. M. Hörl, Acta Crystallogr. **15**, 845 (1962).

[47] C. Elsasser, K. M. Ho, C. T. Chan, and M. Fahnle, J. Phys.: Condens. Matter **4**, 5207 (1992).

[48] D. K. Ross, *Hydrogen in Metals III* (Springer, Berlin, 1997), p. 184.